CHARACTERIZING ERROR IN PEAK SKIN DOSE CALCULATIONS FOR FLUOROSCOPICALLY GUIDED INTERVENTIONS

By

Grace E. Eliason

A THESIS

Presented to the Oregon Health & Science University
School of Medicine
in partial fulfillment of
the requirements for the degree of

MASTER OF SCIENCE

June 2021

TABLE OF CONTENTS

List of Figures

List of Tables

Abbreviations

BSF	Backscatter factor
DAP	Dose-area product
DSA	Digital subtraction angiography
FGI	Fluoroscopically guided intervention
FOV	Field of view
Gy	Gray
HVL	Half-value layer
IRP	Interventional reference point
K_a	Air kerma
$K_{a,r}$	Air kerma at the interventional reference point
kVp	Peak kilovoltage
OHSU	Oregon Health and Science University
OR	Operating room
OSLD	Optically stimulated luminescent dosimeter
PACS	Picture archiving and communication system
PSD	Peak skin dose
RDSR	Radiation dose structured report
SRDL	Substantial radiation dose level
TAF	Table attenuation factor

Acknowledgements

I would first like to express immeasurable gratitude to my mentor, Dr. Anna Mench, for the hours of work she has committed to this research project. From the many bunny-suited evenings spent in the OR to carefully reading nanoDots *ad nauseum*, the scope of this work would not have been remotely achievable without her time input. In addition, the resources she made available to me are appreciable and appreciated. Thank you to her family for coping with her abnormal work hours; I will try my best to regulate our research schedule as I continue as a resident at OHSU.

I would also like to thank Dr. Celeste Leary for developing the voxelized phantom used in our MATLAB PSD calculation program; this work would have been all for naught without her quaternion witchcraft. Moreover, I, along with my graduate cohort, would like to thank Dr. Leary for being the shining light at the end of a dark, intimidating tunnel. We all aspire to be as dedicated a student, as competent a medical physicist, and as compassionate a person as she is. I truly won the lottery when it comes to senior residents.

Next, I would like to acknowledge my committee members for their guidance throughout this project and my graduate studies at OHSU. Dr. Lindsay DeWeese challenges me as a student, researcher, and clinical physicist, trusting my process and critiquing me justly. She has always empowered me to take an active role in my education and career, and I look forward to more of her wisdom as my residency director. Susha Pillai created a welcoming space for me, an imaging physics student, in the radiation therapy department

at OHSU and acted as our clinical-use nanoDot expert for this project. I know that I will always be able to depend on her for physics resources or for nostalgic chit-chat about Nebraska.

Thank you to OHSU-favorite Thai Yummy food cart for fueling many data collection evenings. Thank you also to the OHSU aerial tram conductors for their consistency and kindness on days when I had neither nor. Thank you to hospital workers and vendors, especially those who in OR 25 and Cath Lab 3 and those who work for Philips and Siemens.

Thank you to my family for humoring me when I discussed my research and for keeping me grounded throughout my educational journey. I delighted in the video-chats we had during the pandemic and jumped for joy at every video of my sweet baby niece and goddaughter.

Finally, thank you to my fiancé, Russell McFarland, for encouraging me to do research during undergraduate. Without you pushing me, I never would have known what I am capable of.

Abstract

Purpose: For fluoroscopically guided interventions (FGIs) that reach substantial radiation dose levels, NCRP Report No. 168 recommends estimating peak skin dose (PSD) to evaluate possible radiation-induced skin injuries. Oregon Health and Science University (OHSU) currently employs dose-monitoring software Imalogix™ to display dose metrics and calculate PSD for each sent FGI. The variables in a PSD calculation include air kerma at the interventional reference point ($K_{a,r}$), backscatter factor (BSF), table attenuation factor (TAF), tissue-conversion factor (f), and distance correction factor. In their piecewise Java™-based PSD calculation, Imalogix sets their BSF and TAF to 1.3 and 0.75, respectively, and $K_{a,r}$ values come from on-unit dose area product (DAP) meters. The intent of this project was to measure these variables and employ corrections to minimize errors in a PSD calculation.

Methods: Measurements for BSF and TAF were made on Philips Allura and Siemens Artis Q fluoroscopy units using a RTI T20 Dose Probe in conjunction with an RTI Magna 1cc ion chamber. Acrylic blocks were used as the scattering medium for BSF measurements. K_a meter accuracy was investigated with a metadata analysis of annual physics reports. BSF, TAF, and $K_{a,r}$ measurements were then implemented into an in-house PSD calculation program. Simulated exams were then performed on an anthropomorphic chest phantom with an inset skeletal system during which nanoDot™ optically simulated luminescent dosimeters (OSLDs) directly measured PSD. The in-house PSD calculator was then compared to Imalogix and to direct dosimetric measurements on an anthropomorphic phantom.

Results: BSF ranged from 1.06 to 1.77 depending on acrylic phantom thickness, field size, and fluoroscopic unit; TAF ranged from 0.34 to 0.89 depending on table pad and patient-positioning gel used. $K_{a,r}$ meter accuracy on interventional fluoroscopic units at OHSU ranged from 33.07% and +26.90% in the 2020 testing year and –21.46% and +33.07% in the 2021 testing year. The in-house PSD calculator correlated with Imalogix by approximately 0.7 when the same inputs were used. The in-house PSD calculator was nearest to nanoDot measurements using 2021 $K_{a,r}$ meter accuracy and measured BSF and TAF values.

Conclusions: Simple inputs such as $K_{a,r}$ meter percent error could improve PSD calculation accuracy by upwards of 50%. More complex inputs, such as BSF and TAF, warrant literature-informed approximations and should be adjusted per irradiation event or on a unit-by-unit basis. Variables employed in PSD calculations should be investigated prior to performing patient-specific calculations to minimize error and inconsistent patient follow-up recommendations.

1. Introduction

1.1. Fluoroscopically guided interventions (FGIs)

Fluoroscopically guided interventions (FGIs) are defined by NCRP Report No. 168 as "diagnostic or therapeutic interventional medical procedures performed via percutaneous or other access routes"; this includes but is not limited to procedures such as embolization, biopsy, device placement, and ablation [1]. These procedures are becoming more prevalent due to their less-invasive nature. In 2013, 4.06 million cardiac catheterization lab procedures were performed in the U.S. alone, which represents a 1.7% average annual increase since 2008 [2].

An FGI procedure is considered to have a potentially high radiation dose if more than 5% of cases result in a cumulative air kerma (CAK) exceeding 3 Gray (Gy) or a dose-area product (DAP) exceeding 300 Gy cm^2 [1]. In some cases, these procedures can accrue CAKs greater than 5 Gy and beam-on times greater than 1 hour. Because of this, radiation-induced skin injuries are known to be potential complications of FGIs [1]. It is important to note that although FGIs surpass these dose metrics only a small fraction of the time, any radiation injury will seriously impact the patient's quality of life.

1.2. FGI dose reporting

In order to monitor radiation dose to patients undergoing FGIs, NCRP 168 has defined a Substantial Radiation Dose Level (SRDL) as a fluoroscopy time greater than or equal to

60 minutes, a dose-area product (DAP) greater than or equal to 500 Gy cm^2, a CAK greater than or equal to 5 Gy, or a peak skin dose (PSD) greater than or equal to 3 Gy [1].

These values as well as first notifications are summarized in Table 1. If an SRDL is reached, NCRP 168 recommends the interventionalist place a note and justification in the medical record immediately post-procedure, inform the patient of possible deterministic effects, and follow-up with the patient for at least one year post-procedure [1].

Metric	First Notification	SRDL
Fluoroscopy time	30 min	60 min
Dose area product (DAP)	300 Gy cm^2	500 Gy cm^2
Cumulative air kerma (CAK)	3 Gy	5 Gy
Peak skin dose (PSD)	2 Gy	3 Gy

Table 1. Dose metrics and levels to monitor in FGIs according to NCRP 168.

As of 2006, air kerma at a reference point ($K_{a,r}$) approximately near the patient's skin entrance must be displayed in real time on all fluoroscopes [3,4]. For most C-arm fluoroscopes, the interventional reference point (IRP) is 15 cm from isocenter toward the x-ray tube along the central axis of the beam [3,5]. Along with cumulative air kerma (CAK), cumulative DAP and fluoroscopy time are displayed on almost all modern units. All dosimetric information is documented in the patient's medical record at the conclusion of each procedure as a Radiation Dose Structured Report (RDSR) [5,6]. On-unit meters create and send these RDSRs directly to PACS; they are organized by individual irradiation event and include x-ray tube techniques, tube positioning data, table positioning data, and measured $K_{a,r}$. Total RDSR metrics and metrics per Irradiation

Event are shown in Table Table ***2***. *Exam total RDSR headers for a Philips Allura stationary C-arm.* and Table Table ***3***, respectively.

RDSR Header	Unit
Dose Area Product Total	Gy.m2
Dose (RP) Total	Gy
Fluoro Dose Area Product Total	Gy.m2
Fluoro Dose (RP) Total	Gy
Total Fluoro Time	s
Acquisition Dose Area Product Total	Gy.m2
Acquisition Dose (RP) Total	Gy
Total Acquisition Time	s
Total Number of Radiographic Frames	
Height of System	mm
Focal Spot to ISO Center	mm

Table 2. Exam total RDSR headers for a Philips Allura stationary C-arm.

RDSR Subheader	Unit
DateTime Started	
Irradiation Event Type	
Dose Area Product	Gy.m2
Dose (RP)	Gy
Positioner Primary Angle	deg
Positioner Secondary Angle	deg
X-Ray Filter Material	mm
X-Ray Filter Thickness	mm
X-Ray Tube Current	mA
Distance Source to Isocenter	mm
KVP	kV
Pulse Width	ms
Irradiation Duration	s
Patient Table Relationship	
Patient Orientation	
Table Longitudinal Position	mm
Table Lateral Position	mm
Target Region	
Final Distance Source to Detector	mm
Final Table Height Position	mm
Detector Field Size (X side/Y side)	mm
Object Thickness	mm

Table 3. Irradiation Event RDSR headers for Philips Allura stationary C-arm.

1.3. FGI dose metrics

Dose metrics such as CAK and DAP are recommended by NCRP 168 only to compare similar FGI procedures for possible outliers [1]. Both of these metrics only take dose to air at the IRP and field size into account, ignoring backscatter, table attenuation, and patient position relative to the beam. In addition, although an alarm sounds after 5 minutes of beam-on time, fluoroscopy time should not be used as the only dose indicator during an FGI [1]. Instead, more meaningful dose metrics should be used.

In order to evaluate possible deterministic effects, NCRP 168 recommends PSD as a dose metric above other available dose metrics [1]. This is because PSD is a value that corrects CAK for distance to patient, field size, backscatter, table attenuation, and material, e.g. tissue. Unfortunately, PSD is a calculated value and as such is not currently displayed in real time, forcing interventionalists to rely on the other three dose metrics during the procedure.

1.4. Dose monitoring at OHSU

Oregon Health and Science University (OHSU) employs dose monitoring platform Imalogix™ to monitor exam-specific patient dose and dose trends for CT and fluoroscopy exams. After all fluoroscopy procedures, DICOM headers and radiation dose structured reports (RDSRs) are sent through PACS to Imalogix cloud-based system. Imalogix reports several parameters, including CAK, DAP, and fluoroscopy time, and also calculates PSD based on the method from Jones and Pasciak [7]. The dose

monitoring software has created a Java™-based program which positions the patient relative to the beam by inputting RDSR data onto a voxelized cylindrical phantom. This distance and area correction is applied to the unit-reported $K_{a,r}$, literature-informed BSF and TAF values of 1.3 and 0.75, respectively, and well-established air-to-tissue conversion factors between 1.065 and 1.100.

OHSU sets dosimetric values for which exams are flagged for review on Imalogix. As of 2021, Level II Alerts at OHSU are PSD or a CAK values greater than or equal to 5 Gy per fluoroscopic procedure. These values were chosen based on recommendations from NCRP 168, however, the PSD limit is significantly greater than the SRDL of 3 Gy. This is because OHSU has yet to benchmark Imalogix reported PSD with their own calculated PSD, and neither has been verified with direct dosimetric measurements. Cases in which the PSD is overestimated then flagged may lead to unnecessary follow-up and undue stress on both the patient and the interventionalist; cases in which the PSD is underestimated then left unflagged may result in unchecked deterministic effects.

1.5. Specific Aims

The primary goal of this study was to compare an in-house PSD calculation to that of Imalogix dose monitoring software and to OSLD measurements of simulated FGI procedures. With this goal came five specific aims:

1. Measure ground-truth $K_{a,r}$, TAF, and BSF values of frequently used fluoroscopic units at OHSU for reference when calculating PSD in-house and for exploring the range of error in Imalogix PSD calculation.

2. Develop an in-house PSD calculator using measured $K_{a,r}$, TAF, and BSF values as well as an ellipsoidal phantom and literature-established tissue conversion factors.
3. Simulate FGI procedures on anthropomorphic phantoms while taking direct dosimetric measurements with nanoDot™ OLSDs to test the accuracy both the aforementioned in-house PSD calculations and Imalogix PSD calculations.
4. Perform a retrospective analysis using clinical RDSR data to test the in-house PSD calculator to Imalogix with identical inputs.
5. Test the in-house PSD calculator to aforementioned OSLD measurements with measured $K_{a,r}$, BSF, and TAF inputs.

2. Background

2.1. Peak skin dose (PSD)

Outlined by Jones and Pasciak[7], the PSD calculation employed by Imalogix is given piecewise as the following:

$$\mathrm{PSD} = \sum_{\mathrm{exam}} K_{\mathrm{air,IRP}} \times \mathrm{BSF} \times \mathrm{TAF} \times f \times \left(\frac{d_{\mathrm{source-IRP}}}{d_{\mathrm{source-patient}}} \right)^2$$

where $K_{air,IRP}$ is the air kerma at the interventional reference point ($K_{a,r}$), BSF is the backscatter factor, TAF is the table attenuation factor, f is the tissue-conversion or f-factor, and the final term is the distance correction or inverse-square factor (ISF). Both Imalogix and the in-house PSD calculator, developed in MATLAB, take a piecewise approach to the calculation, extracting data per Irradiation Event from the RDSR; this is shown as the summation symbol in the calculation above. Each of the variables in this PSD calculation are explained in the following subsections.

2.1.1. Air kerma ($K_{a,r}$)

Kerma, or KERMA, is an acronym referring to the "Kinetic Energy Released in MAtter"; therefore air kerma at the interventional reference point ($K_{a,r}$) is the kinetic energy released in air, or the radiation dose to air, at a defined point in space. As of 2006, the FDA and IEC require $K_{a,r}$ to be displayed in real time on all C-arm fluoroscopic units, whether it originate from an on-unit $K_{a,r}$ meter or is calibrated based on x-ray techniques. $K_{a,r}$ meter accuracy is tested annually by physicists as outlined by AAPM Task Group Report No. 190 [4,5,8]. Depending upon the unit vendor and model, the reference point is meant to approximate where the beam enters the patient surface or skin. The FDA- and

IEC-compliant interventional reference point (IRP) is 15 cm from isocenter toward the x-ray tube along the central axis of the beam as illustrated in Figure 1 [4,5,8]. Note that the source-image distance (SID) may be increased or decreased by moving the image receptor along the central beam axis, however the IRP is defined with respect to the distance from the source, which remains constant. $K_{a,r}$ meter accuracy is tested annually, and the displayed CAK and DAP are allowed to deviate from their physically measured values at the reference point by up to +/- 35% [4,5].

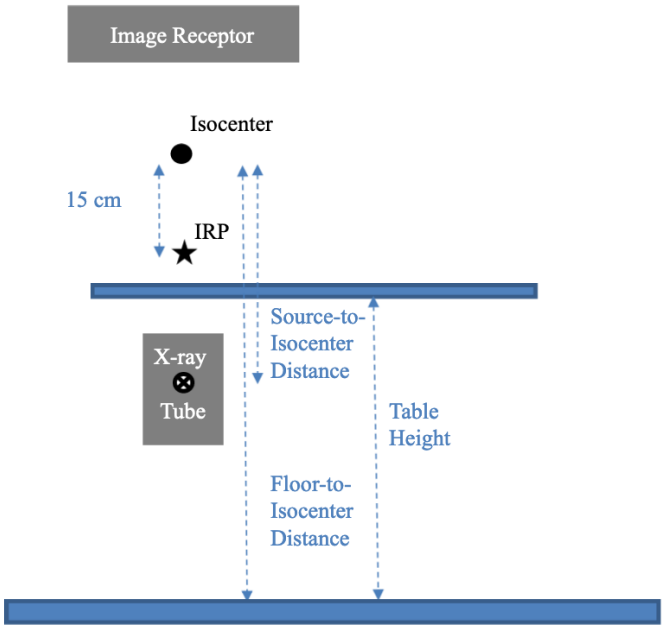

Figure 1. Illustration of the interventional reference point (IRP) with respect to isocenter of a stationary C-arm.

2.1.2. Backscatter factor (BSF)

Radiation dose is imparted to a material through photon interactions with atoms of the material that free or generate charged particles. At certain energies, some interactions are more likely to occur than others. Most x-ray photons, which are at energies between 0

and 120 kV, will undergo photoelectric absorption, where the photon is completely absorbed by the atom. This interaction is the basis for radiographic image formation and can be thought of as a sort of "shadow puppet" effect. Another interaction that can occur in this energy range is Compton scattering. In this interaction, the photon is not fully absorbed by the atom, but instead changes direction and is then considered "scattered". Although less likely than absorption, scattering events such as these do occur during any x-ray exposure. Both photoelectric absorption and Compton scattering contribute to patient dose; Compton scatter's contribution, however, is more heavily weighted toward the beam entrance surface.

In a PSD calculation, backscatter factor (BSF) accounts for this internally created scatter radiation to the patient's surface. For experimental purposes, BSF is defined as the ratio of $K_{a,r}$ on a patient's surface to the same point in-air. All BSFs are above 1.00 and are found to range from 1.15 to 1.58 for diagnostic energies, meaning that scatter contributes 15% to 58% additional radiation dose to the patient surface [9,10]. BSF is a function of x-ray field size, beam quality, beam filtration, and patient thickness [7,9,10]. Generally, BSF will increase for increasing x-ray field size and beam energy, will increase then level-out for increasing patient thickness, and will increase then decrease for increasing beam filtration [7].

2.1.3. Table attenuation factor (TAF)

Table attenuation factor (TAF) accounts for the change in beam quality as it passes through the table and added attenuators prior to reaching the patient. In a clinical

scenario, the most basic set of attenuators in the way of the beam will be the treatment table and pad, with added attenuators such as gel positioning devices underneath the patient in certain cases. These devices lack heavy attenuation materials such as lead, allowing the fluoroscope to produce a clear image of the patient even through the table. Although these materials do not attenuate the beam to the extent that lead does, they do lessen the amount of beam that reaches the patient, lowering the dose to the patient's skin as a result.

From an experimental standpoint, TAF is defined as the ratio of $K_{a,r}$ in the presence of attenuators to the same point in-air. All TAFs are below 1.00 and are found to range from 0.52 to 0.83 in the diagnostic energy range, meaning that the table and pad attenuate between 17% to 48% of the beam before it reaches the patient [9]. TAF is a function of x-ray field size, beam quality, beam filtration, and attenuator type and thickness [9].

2.1.4. f-factor (f)

The tissue-conversion- or f-factor (f) converts dose to air into dose to tissue and is equal to the ratio of mass attenuation coefficients of the medium to air, or

$$f(E) = \frac{\left(\frac{\mu(E)}{\rho}\right)_{\text{tissue}}}{\left(\frac{\mu(E)}{\rho}\right)_{\text{air}}},$$

where μ is the linear attenuation coefficient of the material at energy E and ρ is the density of the material. The mass attenuation coefficient describes how a medium interacts with incoming photon radiation at a given energy; at the energies used in fluoroscopy, between 60 and 120 kVp, the dominating photon interaction is photoelectric

absorption. F-factors are well-established in the literature and range from 1.056 to 1.069 in the diagnostic energy range [7]. The f-factor is a function of x-ray beam quality [8].

2.1.5. Distance correction

The inverse-square factor (ISF) or distance correction converts $K_{a,r}$ at the IRP to $K_{a,r}$ at the patient surface closest to the x-ray tube. This correction is a consequence of the intensity of a beam decreasing as $1/r^2$ with increasing distance or radius (r) from the source, or

$$\mathrm{ISF} = \left(\frac{d_{\mathrm{source-IRP}}}{d_{\mathrm{source-patient}}} \right)^2 .$$

The ISF will be greater than 1.00 for a patient surface between the x-ray tube, or source, and the IRP and lesser than 1.00 for a patient surface farther from the tube than the IRP.

2.2. Optically stimulated luminescent dosimeters (OSLDs)

Optically stimulated luminescent dosimeters, or OSLDs, collect and store radiation dose information similar to that of a semiconductor diode. Dopants in the crystal lattice act as electron trapping sites between the conduction and valence energy bands. When exposed to radiation, an electron-hole pair is created; as the electron attempts to recombine with this hole, it becomes energetically “stuck” in the bandgap between the bands in one of these electron traps. Many electrons can be captured by a single trap until the trap becomes saturated; the saturation of captured electrons is proportional to the exposure. Radiation dose information is stored in the OSLD until readout.

The readout process of an OSLD is as the name implies. Electrons stored in the trapping centers become released when exposed to light. The energy of light required to release these electrons is equal to the difference between the trap and the band; subsequently, when this electron is released, the energy imparted by the light is greater than that required for the electron to recombine with its hole. This excess energy is released as a photon at a lower energy than the stimulation photon. The separation between simulation and readout energies allows for signal filtration. A photomultiplier tube converts these readout photons into electrons and then amplifies the signal to be read as a current proportional to the originally absorbed dose.

Much like inorganic scintillators, OSLDs must be in solid form to measure radiation dose, as the electron traps are inherent to their crystalline structure. An advantage to this lattice approach is that OSLDs can reliably measure radiation dose in smaller form factors. Additionally, while the radiation dose measurement and storage technique is identical to that of thermoluminescent dosimeters, OSLDs can be read multiple times after an exposure. Common applications of OSLDs include personnel dosimetry, patient skin dose verification in radiation therapy, and medical physics dosimetry research.

3. Methods and Materials

3.1. PSD variables

3.1.1. Air kerma ($K_{a,r}$)

For both dose metric reports and PSD calculations, Imalogix extracts the unit-reported CAK and DAP values directly from the RDSR, not taking $K_{a,r}$ meter inaccuracy into account. A metadata study of $K_{a,r}$ meter accuracy from all 2020 and 2021 annual physics reports at OHSU was performed in order to evaluate the overall scope of inaccuracy and to input unit-specific error into the in-house PSD calculator.

$K_{a,r}$ meter-accuracy measurements were performed by a number of physicists at OHSU as per the recommendations of TG-190, in which in-air measurements are taken with an external detector at the IRP and unit-displayed air kerma is recorded [8]. The percent error is then given as the difference between these two values divided by the ground truth measurement, or that of an external detector. The external detector used in these measurements was one of two Piranha T20 dose probes connected to a Piranha base unit. The $K_{a,r}$ meter percent error implemented into the in-house PSD calculator was that of the 2021 testing year.

3.1.2. Backscatter factor (BSF)

Imalogix uses a constant BSF of 1.3 in their piecewise PSD calculations independent of x-ray techniques provided in the RDSR. The in-house PSD calculation will interpolate from a set of unit-specific measured BSF values as a function of techniques for each Irradiation Event.

A lateral-tube method was used to measure exposure rates as illustrated in Figure 2. Illustration of the backscatter factor (BSF) lateral-tube measurement method. . The ratio of phantom-present to phantom-absent exposure rates was taken to be the BSF for a given phantom thickness, field-of-view (FOV), additional beam filtration (mmCu), and set kilovoltage (kVp). Source-to-meter distance needed to be consistent between individual sets of measurements but could be adjusted for exposure rates to fall within meter limits. All measurements were performed over several sessions on a Philips Allura and a Siemens Artis Q stationary C-arms, the former being a single-plane and the latter a biplane wherein only the frontal tube was used. Exposure rate measurements were taken using a Piranha T20 solid-state, backscatter-protected dose probe as well as a Piranha Magna 1-cc ion chamber. Details on the fluoroscopic units as well as the measurement tools are provided in Section 3.2.

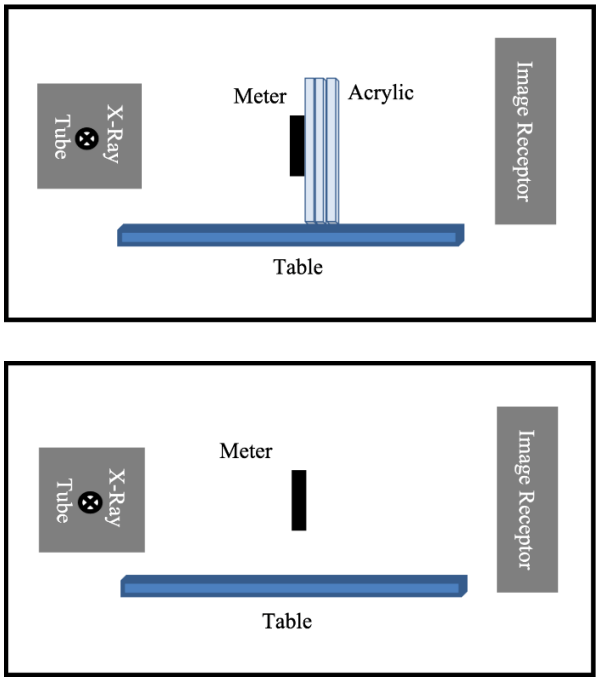

Figure 2. Illustration of the backscatter factor (BSF) lateral-tube measurement method.

3.1.3. Table attenuation factor (TAF)

Imalogix uses a constant TAF of 0.75 in their piecewise PSD calculations, unless the primary beam does not pass through the table for a given Irradiation Event, in which case they set it equal to 1. The in-house PSD calculation will employ measured TAF values for each unit explored, unless the primary beam does not pass through the table for a given Irradiation Event, in which TAF will be set equal to 1. From measurements performed on the C-arms examined, the angle at which TAF is set to 1 is 60 degrees along the rotational axis of the C-arm.

A frontal-tube P-A method was used measure exposure rates as illustrated in Figure 3. Illustration of the table attenuation factor (TAF) frontal-tube measurement method.. The ratio of attenuator-present to attenuator-absent exposure rates was taken to be the TAF for a given set of attenuators, including table, table + pad, and other additional patient positioning devices. Variables such as FOV, mmCu, and kVp were kept constant. All measurements were performed over several sessions on a Philips Allura and a Siemens Artis Q stationary C-arms, the former being a single-plane and the latter a biplane wherein only the frontal tube was used. Exposure rate measurements were taken using a Piranha T20 solid-state, backscatter-protected dose probe as well as a Piranha Magna 1-cc ion chamber. Details on the fluoroscopic units as well as the measurement tools are provided in Section 3.2.

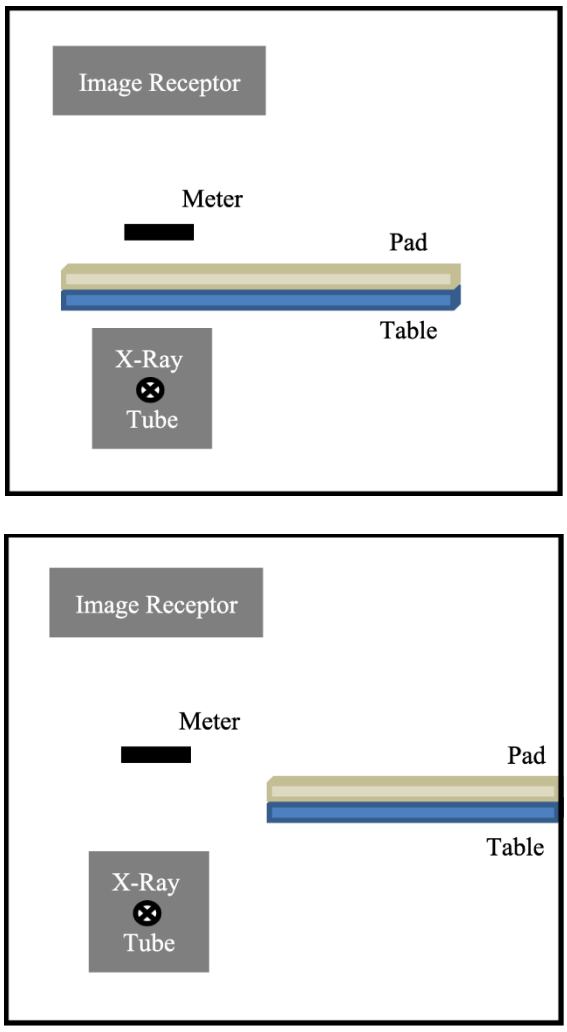

Figure 3. Illustration of the table attenuation factor (TAF) frontal-tube measurement method.

3.1.4. f-factor (f)

Imalogix interpolates an f-factor between 1.065 to 1.100 based on a kVp for each Irradiation Event in the RDSR. Values used for f-factor were interpolated from Table 4 of Jones & Pasciak as a function of kVp and acquisition type for each Irradiation Event [7].

3.1.5. Distance correction

Both Imalogix and the in-house PSD calculator take positional RDSR data, listed in Table 3, places a voxelixed phantom on the table surface, and creates an intensity map of distance corrections per Irradiation Event. In addition to distance, both Imalogix and the developed PSD programs take geometry into account, recreating the field size as it enters the patient. Imalogix voxelized phantom is programmed in Java™ as a right cylinder with a 30-cm diameter. The voxelized phantom used in the developed PSD calculator is programmed in MATLAB as an ellipsoidal cylinder where the minor axis is set to the Object Thickness provided in the RDSR and the major axis is set the 1.3 times the Object Thickness. If the RDSR does not provide an Object Thickness metric, as is the case with the Siemens Artis Q unit, the Object Thickness is set to 30 cm.

3.2. Equipment

3.2.1. RTI dose meters

Figure 4. Photograph of RTI dose meters used for BSF and TAF measurements.

3.2.1.a. RTI Piranha base unit

The RTI Piranha base unit, pictured in the center of Figure 4, is an electrometer-detector combination that connects via Bluetooth or USB to a PC. The internal detector is a backscatter-protected solid-state meter with a detector area of 3 mm by 21.1 mm and is capable of measuring tube voltage (kVp), exposure time, dose, dose rate, beam filtration, beam half-value layer (HVL), kVp waveform, and dose rate waveform [11]. Detectable doses and dose rates per run are 0.7 µGy – 650 Gy and 10 µGy/s – 320 mGy/s, respectively; operating temperatures and air pressures are 15-35 °C and 80-106 kPa, respectively [11]. The external probes connected to the Piranha base unit during this experiment were the RTI T20 dose probe and the RTI Magna 1cc ion chamber. Both internal and external meters can be read simultaneously using Ocean™ QA software. For the purposes of these experiments, the base unit was used primarily as a Bluetooth connection for the external meters and secondarily as a means of measuring beam HVL. This meter was calibrated for air kerma by an accredited calibration laboratory on 08/19/2020 and as such does not require recalibration until 08/18/2022.

3.2.1.b. RTI T20 dose probe

The RTI T20 dose probe, pictured on the left in Figure 4, is an external meter that connects via triaxial cable to the RTI Piranha base unit. The detector is a backscatter-protected PIN semiconductor diode with an active area of 6 mm by 35 mm and is capable of measuring tube voltage (kVp), exposure time, dose, dose rate, beam filtration, beam HVL, kVp waveform, and dose rate waveform [11,12]. Detectable doses and dose rates per run are 700 pGy - 10 kGy and 27 nGy/s - 500 mGy/s, respectively; operating

temperatures are 18-23°C at less than 80% relative humidity [12]. For the purposes of these experiments, the T20 was used primarily as a means of measuring exposure rate when the RTI Magna 1cc ion chamber was unavailable and secondarily as a backscatter-protected comparison to the RTI Magna 1cc ion chamber. This meter was calibrated for air kerma by an accredited calibration laboratory on 08/19/2020 and as such does not require recalibration until 08/18/2022.

3.2.1.c. RTI Magna 1cc ion chamber

The RTI Magna 1cc ion chamber, pictured on the right in Figure 4, is an external meter that connects via triaxial cable to the RTI Chamber Adapter which connects to the Piranha base unit. The detector is a backscatter-unprotected gas ionization chamber with an active volume of 1 cm^2 and is capable of measuring exposure time, dose, and dose rate [11,13]. Detectable dose rates per run when connected to the RTI Chamber Adapter are 0.25 mGy/s - 2.5 Gy/s; operating temperatures are 18-23°C at less than 80% relative humidity [13]. For the purposes of these experiments, the Magna 1cc ion chamber was used primarily as a means of measuring exposure rate. This meter was calibrated for air kerma by an accredited calibration laboratory on 08/19/2020 and as such does not require recalibration until 08/18/2022.

3.2.2. Landauer nanoDot™ OSLDs and microSTAR®ii reader

3.2.2.a. nanoDot energy correction measurements

Landauer's nanoDot™ optically stimulated luminescent dosimeters (OSLDs) and microSTAR®ii medical dosimetry system is designed for patient dose verification or

quality control dosimetry [14,15]. For the latter implementation, all nanoDot OSLDs can be reused by bleaching the active component between dose exposures and readouts. The hardware components include the microSTARii reader, a set of Calibration nanoDots, a set of QC nanoDots, a barcode scanner, and a provided laptop with a software application for operating the reader, managing data, and reporting dosimetry results [14,15]. The system can be used for therapeutic or diagnostic applications, the calibration energies for which are Cs-137 and 80 kVp, respectively. The 80 kVp Calibration kit was performed in January 2021 by the authors.

The active element in a nanoDot is a 5-mm-wide, 0.3-mm-thick cylindrical disk of aluminum oxide doped with carbon (Al_2O_3 :C) embedded in a square plastic case 10-mm wide and 2-mm thick; the QR code and last few digits of the nanoDot serial number are displayed on the plastic case [15]. The detectable dose range by each nanoDot is 50 µGy - 1500 cGy, and the recommended operating temperature is 65 °F - 75 °F in less than 80% relative humidity. Each nanoDot can be read multiple times post-exposure with minimal depletion, and signal fade is estimated to be 1% per calendar quarter. Two sets of 50 screened nanoDots each were utilized during this experiment; the background of each was read prior to exposure and after bleaching. Daily quality control tests were performed on the microSTARii reader prior to every nanoDot readout session. The absorbed dose is calculated by subtracting the background counts from the raw counts and dividing that value by the 80 kVp calibration factor, measured in counts per dose, and individual nanoDot sensitivity, a unitless factor provided by the manufacturer. Each nanoDot was read four times for reproducibility.

OSLDs display an energy dependence at diagnostic energies. Though this dependence is on the order of +/- 10 %, a calibration curve was generated for energies for 60 to 120 kVp in 5 kV increments for improved accuracy. For these measurements, the Philips Allura unit was set to service mode with an SID of 100 cm and a FOV of 48 cm, and exposures were taken at 120 mA for 500 ms. Each run was comprised of four nanoDots directly facing the x-ray tube placed in a 2x2 grid, as shown in Figure 5.

Figure 5. Photograph of the experimental setup for nanoDot diagnostic energy calibration.

3.2.2.b. nanoDot anthropomorphic phantom measurements

Experimental measurements were taken by placing four to nine nanoDots on an anthropomorphic phantom in a 1x4 line or 3x3 grid, respectively, as shown in Figure 6. All nanoDots were placed at the x-ray beam entrance surface on an anthropomorphic chest phantom; an anthropomorphic pelvis phantom was abutted to the chest phantom to simulate a patient. The chest phantom has maximum anterior-posterior and lateral measurements of 24 cm and a length of 40 cm. The 4x1 nanoDots were placed along the

spine 10-, 5-, and 10-cm apart, and the 3x3 nanoDots were placed approximately 4-cm apart. The 1x4 run tested table motion in fluoroscopy mode in the anterior-poster plane (FL-AP-TAB). The 3x3 runs tested changing FOV in the following mode-position combinations: fluoroscopy AP (FL-AP), digital subtraction angiography AP (DSA-AP), fluoroscopy lateral (FL-LAT), and digital subtraction angiography lateral (DSA-LAT). All experiments were performed on a Siemens Artis Q fluoroscopic unit in automatic exposure rate control (AERC) mode. Each run was used to create a dose distribution map to compare to in-house PSD calculation of RDSR data.

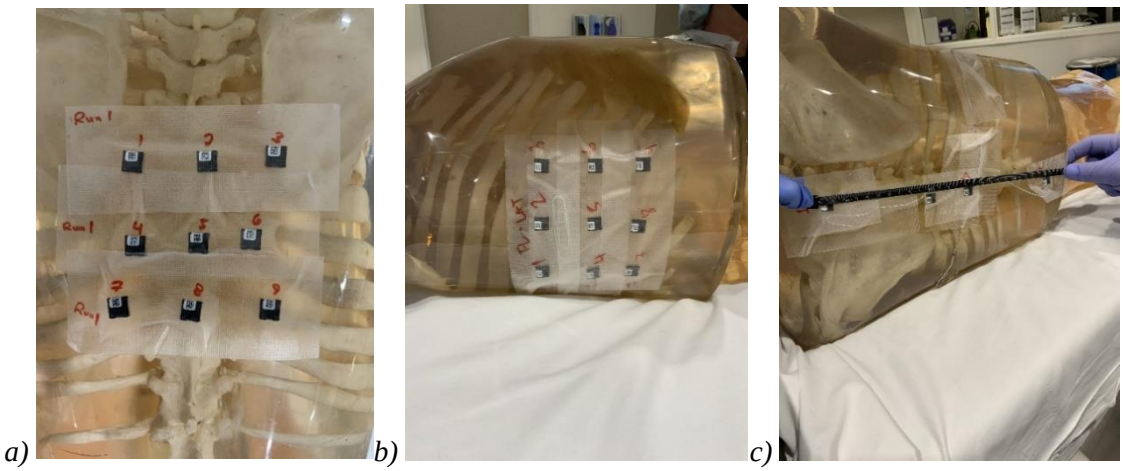

Figure 6. Photographs of experimental setups for nanoDot measurements on an anthropomorphic phantom.
a) Close-up of 9x9 grid in the AP plane corresponding to FL-AP and DSA-AP runs. Phantom chest placed spine-side-down to simulate supine patient position.
b) Side view of 9x9 grid in the LAT plane corresponding to FL-LAT and DSA-LAT runs. Phantom chest placed spine-side-down to simulate supine patient position.
b) Side view of 1x4 grid in the AP plane corresponding to the FL-AP-TAB run. Phantom chest placed spine-side-down to simulate supine patient position.

3.2.3. Fluoroscopic units and ancillary equipment

3.2.3.a. Philips Allura

The Philips Allura used in this experiment is a single-plane, stationary C-arm located in a hybrid operating suite at OHSU. This fluoroscopic unit is equipped with a flat-panel detector (FPD) and all techniques, including additional filtration, are controlled by the on-unit AERC with fluoroscopy protocols chosen by the user. Additional copper filtration is 0.1- and 0.4 mmCu, which correspond to digital acquisition and fluoroscopic modes, respectively. The unit is not used for all procedures in this suite; the FGIs most often performed are labeled Cath Lab Procedures. The unit passed annual testing by an in-house physicist on 3/26/2021. Both TAF and BSF measurements were taken on this unit, as well as nanoDot measurements for the energy calibration curve. Anthropomorphic phantom-nanoDot runs were not performed on this unit.

3.2.3.b. Siemens Artis Q

The Siemens Artis Q used in this experiment is a biplane, stationary C-arm located in a cardiac catheterization lab at OHSU. This fluoroscopic unit is equipped with a flat-panel detector (FPD) and all techniques, including additional filtration, are controlled by the on-unit AERC with fluoroscopy protocols chosen by the user. Additional copper filtration ranges from 0.1- to 0.9 mmCu with is 0.3-, 0.6-, and 0.9-mmCu being the most clinically applied. The unit passed annual testing by an in-house physicist on 3/12/2021. Both TAF and BSF measurements were taken on this unit, as well as anthropomorphic phantom-nanoDot runs, all using the frontal tube.

3.2.4. Phantoms

3.2.4.a. Acrylic sheets

Fourteen acrylic sheets were used to simulate varying patient thickness for the purpose of measuring BSF. Each square sheet has a thickness of 1 inch. The approximate conversion factor to patient thickness is 0.943 [9]. Tested thicknesses were 10-, 12-, and 14 inches of acrylic, which correspond to 23-, 29-, and 33 cm patient thicknesses, respectively. The investigated acrylic thicknesses were meant to reflect typical patient sizes for FGI procedures performed in these rooms. Because the anthropomorphic phantom is 24 cm in diameter, the 10-inch acrylic BSFs were used in the in-house PSD calculator.

3.2.4.b. Anthropomorphic phantom

The phantom applied in the in-house PSD calculator is an ellipsoidal cylinder; in order to closely match this shape and to best approximate source-skin distances, an anthropomorphic chest phantom with inset skeleton, pictured in Figure 6, was used for nanoDot measurements. The chest phantom has maximum anterior-posterior and lateral measurements of 24 cm and a length of 40 cm; the anthropomorphic pelvis phantom abutted to the chest phantom also had an inset skeletal system. The chest cavity was hollow, likely for lung inserts, and the exact material of the phantom was unknown.

4. Results

4.1. PSD variables

4.1.1. Air kerma

$K_{a,r}$ meter and DAP meter accuracy analyses for OHSU stationary C-arms in the 2020 and 2021 testing years can be found in Figures Figure 7a) and b); changes in $K_{a,r}$ meter accuracy between 2020 and 2021 can be found in Figure Figure 7c). Percent error in these analyses is defined as

$$\%_{\text{error}} = \frac{K_{\text{air,meas.}} - K_{\text{air,disp.}}}{K_{\text{air,meas.}}} \times 100 \quad ,$$

wherein a negative percent error indicates that the unit is reading high and a positive percent error indicates that the unit is reading low. Cumulative air kerma (CAK) percent errors ranged between –33.07% and +26.90% in the 2020 testing year and –21.46% and +33.07% in the 2021 testing year. The Philips Allura unit, labeled OR 25, had a -33.07% error in 2020 and +16.57% error in 2021; the Siemens Artis Q labeled Cath Lab 3, had a 5.00% error in 2020 and –11.30% error in 2021. The X-ray tube serial numbers were identical for OR 25 and non-identical for Cath Lab 3, indicating a tube installation between the 2020 and 2021 testing sessions. Additionally, the testing physicist(s) changed between 2020 and 2021. $K_{a,r}$ correction factors used in the in-house PSD calculator were taken as the inverse of one minus the percent error for each year.

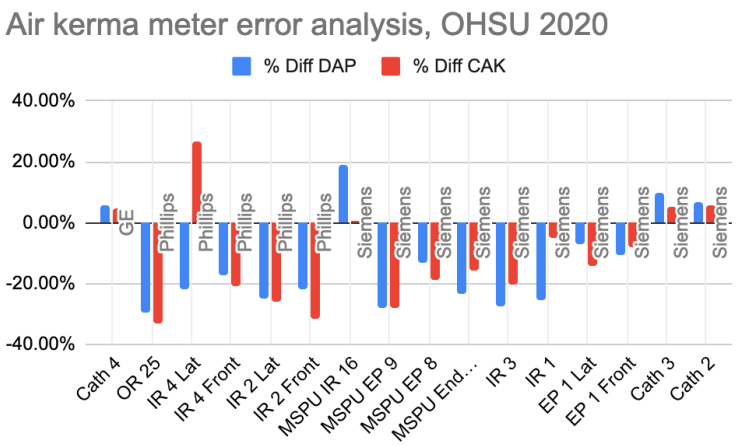

a)

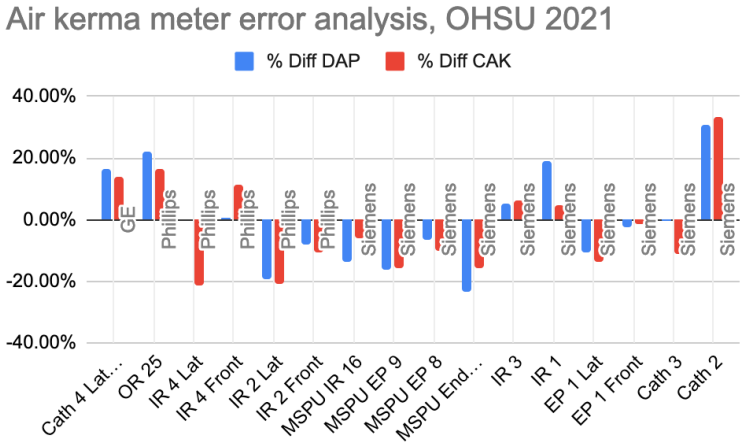

b)

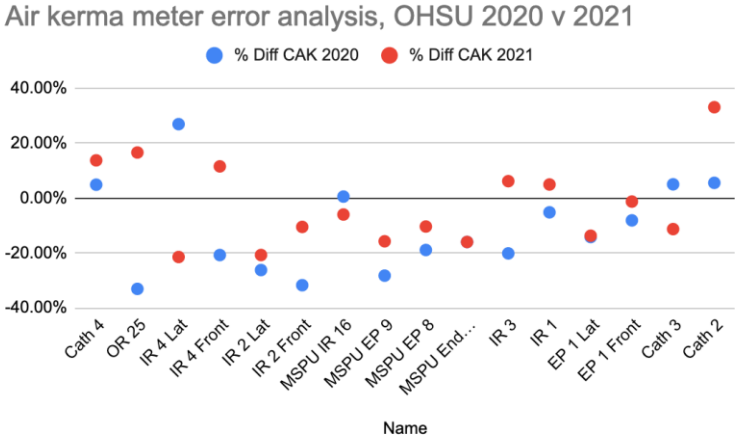

c)

Figure 7. Metadata analysis of air kerma meter accuracy from OHSU annual physics reports in the a) 2020, b) 2021, and c) 2020-2021 testing years.

4.1.2. BSF

4.1.2.a. Philips Allura

BSF values from exposure rate measurements for the Philips Allura unit can be found in Table 4, where BSF is the ratio of acrylic-present to acrylic-absent exposure rate as measured by one or more RTI meters. BSF values ranged from 1.16 to 1.77 and were measured with varying acrylic thicknesses of 10, 12, and 14 inches, x-ray FOVs of 48, 31, and 15 cm, and additional x-ray beam filtration of 0.1 and 0.4 mmCu. N/A value refers to inaccurate meter measurement that resulted in BSF value greater than two. Fluoroscopic and digital acquisition modes were relabeled as copper filtration thicknesses of 0.1 and 0.4, respectively. Exposure rate measurements were taken in service mode with unknown beam filtration. BSFs used in in-house PSD calculator were those at 10 inches of acrylic interpolated by FOV and mmCu data from the RDSR; 10-inch values chosen to match 24-cm anthropomorphic phantom diameter.

		BSF	
Acrylic	**FOV / mmCu**	**0.1**	**0.4**
10 inches	48 cm	1.64	1.77
	31 cm	1.34	1.26
	15 cm	1.16	1.16
12 inches	48 cm	1.39	N/A
	31 cm	1.39	1.41
	15 cm	1.20	1.19
14 inches	48 cm	1.46	1.20
	31 cm	1.37	1.32
	15 cm	1.21	1.19

Table 4. Philips Allura BSF values calculated from exposure rate measurements.

4.1.2.b. Siemens Artis Q

BSF values from exposure rate measurements for the Siemens Artis Q unit can be found in Table 5, where BSF is the ratio of acrylic-present to acrylic-absent exposure rate as measured by one or more RTI meters. BSF values ranged from 1.08 to 1.36 and were measured with varying acrylic thicknesses of 10 and 14 inches, x-ray FOVs of 32 and 22 cm, and additional x-ray beam filtration of 0.3, 0.6, and 0.9 mmCu. Exposure rate measurements were taken in service mode with known beam filtration. BSFs used in in-house PSD calculator were those at 10 inches of acrylic and 80 kVp interpolated by FOV and mmCu data from the RDSR; 10-inch values chosen to match 24-cm anthropomorphic phantom diameter.

			BSF		
Acrylic	**FOV**	**kVp / mmCu**	**0.3**	**0.6**	**0.9**
10	32	80	1.25	1.27	1.26
		100	1.26	1.27	1.27
		120	1.27	1.36	1.27
	22	80	1.14	1.13	1.11
		100	1.13	1.12	1.12
		120	1.13	1.13	1.13
14	32	80	1.06	1.18	1.14
		100	1.07	1.17	1.16
		120	1.08	1.20	1.15
	22	80	1.11	1.10	1.08
		100	1.13	1.11	1.09
		120	1.14	1.14	1.11

Table 5. Siemens Artis Q BSF values calculated from exposure rate measurements.

4.1.3. TAF

4.1.3.a. Philips Allura

TAF values from exposure rate measurements for the Philips Allura unit can be found in Table 6, where TAF is the ratio of attenuator-present to attenuator-absent exposure rate as measured by one or more RTI meters. TAF values ranged from 0.34 to 0.89 and were measured with varying attenuator presence; the clinically applicable TAF value was found to be 0.77 and was measured with just the table and pad. Clinical scenarios require at least table and pad presence, and additional attenuator use is not documented. Only one set of techniques was explored due to the unknown nature of attenuator presence. All measurements taken in clinical mode using AERC.

Material(s)	**Total thickness (cm)**	**kVp**	**mA**	**FOV (cm)**	**Exposure rate (mGy/s)**	**TAF**
In air	0	78	2.7	22	0.0415	
Table	4	78	2.7	22	0.0371	0.89
Table, pad	10	78	2.7	22	0.0319	0.77
Table, pad, arm extender	10.5	78	2.7	22	0.0289	0.70
Table, pad, thin gel	10.5	78	2.7	22	0.0262	0.63
Table, pad, thick gel (inner)	11	78	2.7	22	0.0253	0.61
Table, pad, thick gel (outer)	14	78	2.7	22	0.0142	0.34

Table 6. Phillips Allura TAF values calculated from exposure rate measurements.

4.1.3.b. Siemens Artis Q

TAF values from exposure rate measurements for the Siemens Artis Q unit can be found in Table 7, where TAF is the ratio of attenuator-present to attenuator-absent exposure rate as measured by one or more RTI meters. The clinically applicable TAF value was found to be 0.75 and was measured with just the table and pad. Only one set of techniques was explored due to the unknown nature of attenuator presence. All measurements taken in clinical mode using AERC.

Material(s)	Total thickness (cm)	kVp	mA	FOV (cm)	Exposure (mGy/s)	TAF
In air	0	68.4	156.3	22	0.647	
Table	4	68.4	156.3	22	0.546	0.84
Table, pad	11	68.4	156.3	22	0.487	0.75

Table 7. Siemens Artis Q TAF values calculated from exposure rate measurements.

4.2. nanoDot measurements

4.2.1. nanoDot energy correction measurements

Measurements for the nanoDot energy correction factor were made on the Phillips Allura unit and can be found in Figure 8. Energy correction measurements were made due to the linear response of OSLDs in the diagnostic energy range. Data was collected for energies between 60 and 120 kVp in 5 kVp increments, resulting in minimum and maximum energy correction values of 0.842 and 1.034 from best fit equation:

$$\mathrm{CF} = (0.0032 \times \mathrm{kVp}) + 0.6503$$

.

Measurements were taken on both a T20 dose probe and Magna 1cc ion chamber, and were found to differ by at most 0.9%. The measurements were taken in service mode.

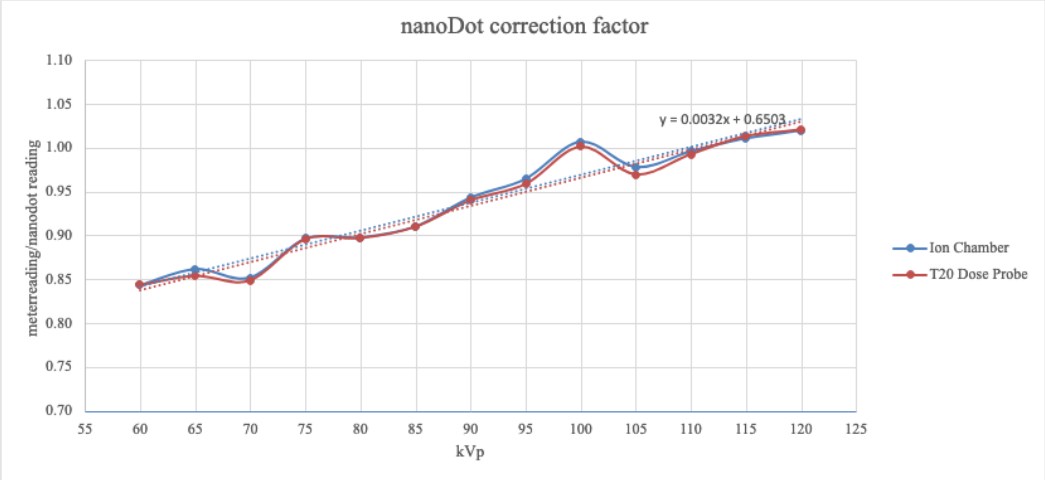

Figure 8. NanoDot energy correction factor for 60 to 120 kVp. All correction factors measured on the Philips Allura stationary C-arm.

4.2.2. nanoDot anthropomorphic phantom measurements

Simulated exams on an anthropomorphic chest phantom were performed on the Siemens Artis Q unit; the nanoDot measurements from these can be seen in Figure 9. Energy-corrected nanoDot dose distribution maps for anthropomorphic phantom runs. . The nanoDot dose distribution maps in were created in MATLAB, where nanoDot locations are displayed as black squares, PSD is indicated in red, and doses between nanodots were interpolated. The nanoDot measurements were corrected for energy using the equation from Figure 8. The kVp for each run was taken as the time-weighted kVp calculated from RDSR data. These time-weighted kVps and their corresponding nanoDot energy correction factors can be found in Table 8. Maximum nanoDot dose measurements, equivalent to PSDs, can also be found in Table 8.

Run	Test	Plane	Mode	kVp	Energy corr. factor	Measured PSD (mGy)
1	FOV	AP	Fluoroscopy	71.2	0.878	6.21
2	FOV	AP	Digital Acquisition	78.0	0.900	4.12
3	FOV	LAT	Fluoroscopy	68.6	0.870	25.75
4	FOV	LAT	Digital Acquisition	76.0	0.894	6.91
5	Table	AP	Fluoroscopy	68.0	0.868	5.43

Table 8. Maximum nanoDot dose measurements for runs on an anthropomorphic phantom

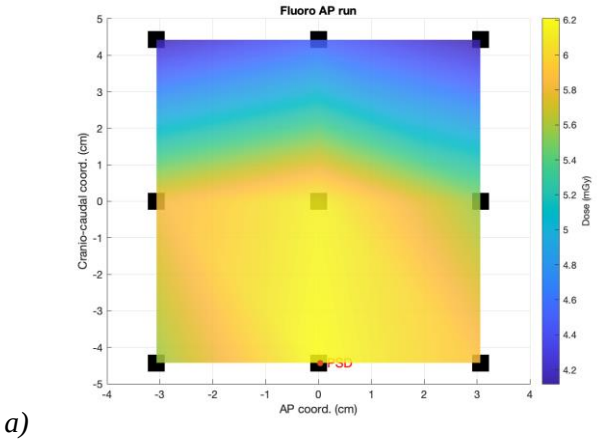

a)

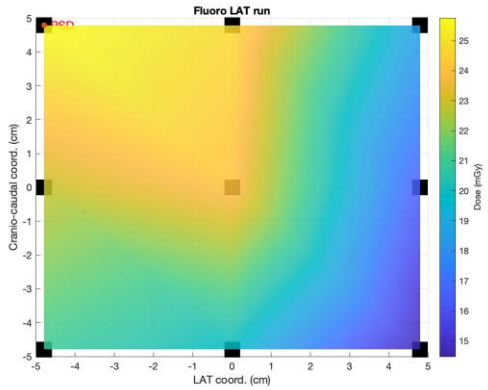

b)

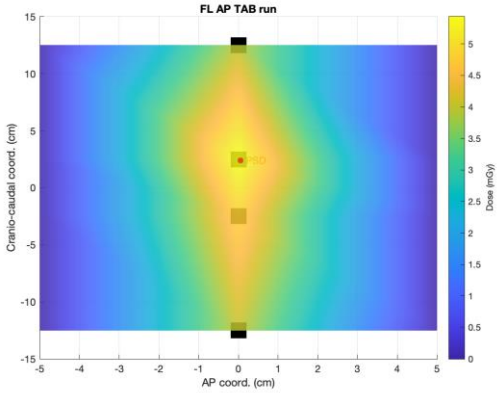

c)

Figure 9. Energy-corrected nanoDot dose distribution maps for anthropomorphic phantom runs.

a) FL-AP run dose map measured by nanoDots; corresponding RDSR-calculated field in Figure 13a.
b) FL-LAT run dose map measured by nanoDots; corresponding RDSR-calculated field in Figure 13b.
c) FL-AP-TAB run dose map measured by nanoDots; corresponding RDSR-calculated field in Figure 13c.

4.3. In-house PSD calculations vs. Imalogix PSD calculations

Retrospective clinical RDSR data was used to compare the in-house PSD calculator to Imalogix and both the CAK; the results of this can be found in Figure 10 and Figure 11. All RDSRs are from March 2020 to March 2021 in OR-25 and Cath Lab 3, which correspond to the Philips Allura and Siemens Artis Q units, respectively. The PSD calculator with $K_{a,r}$, BSF, and TAF values identical to Imalogix is labeled "In-house PSD (Imalogix inputs)" and can be found in Figure Figure 10a); the PSD calculator with corrected $K_{a,r}$, measured BSF values, and measured TAF values is labeled "In-house PSD (measured inputs)" and can be found in Figure Figure 10b). Imalogix and in-house PSD with all corrections are plotted against uncorrected CAK in Figure 11.

In-house PSD with Imalogix inputs resulted in 0.736 and 0.7111 correlations with Imalogix PSD with R^2 fits of 0.828 and 0.968 for the Philips Allura and Siemens Artis Q units, respectively. Using the in-house PSD calculator with measured 2021 $K_{a,r}$ correction factor, BSFs, and TAFs, the Philips Allura increased to 0.865 and the Siemens Artis Q unit decreased to 0.646 correlation with Imalogix.

In-house PSD with Imalogix inputs versus CAK plots, shown in Figure 11a), resulted in slopes of 0.707 and 0.667 with R^2 fits of 0.877 and 0.982 for the Philips Allura and Siemens Artis Q units, respectively. In-house PSD with measured inputs versus CAK plots, shown in Figure 11b), resulted in slopes of 0.831 and 0.605 with R^2 fits of 0.869 and 0.981 for the Philips Allura and Siemens Artis Q units, respectively.

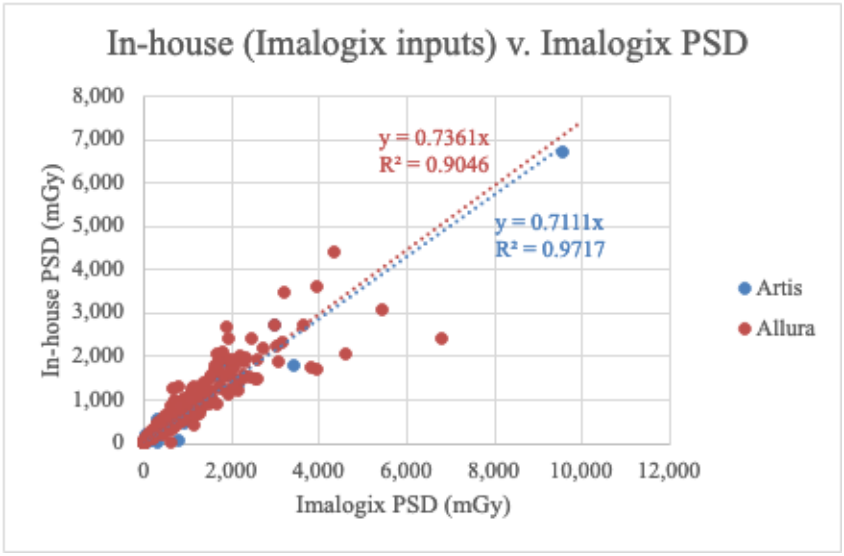

a)

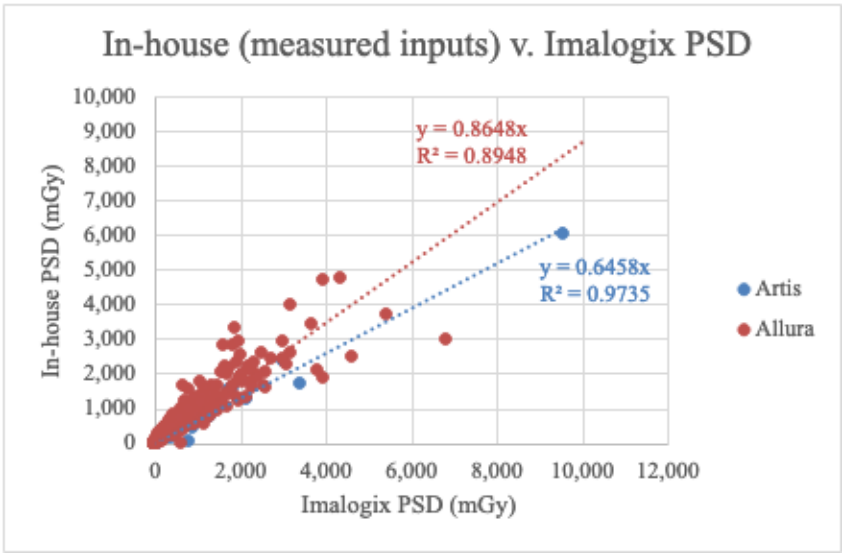

b)

Figure 10. In-house PSD calculations compared to Imalogix PSD calculations using retrospective clinical RDSR data.

a) In-house PSD calculations compared to Imalogix (same inputs)
b) In-house PSD calculations compared to Imalogix (measured inputs)

a)

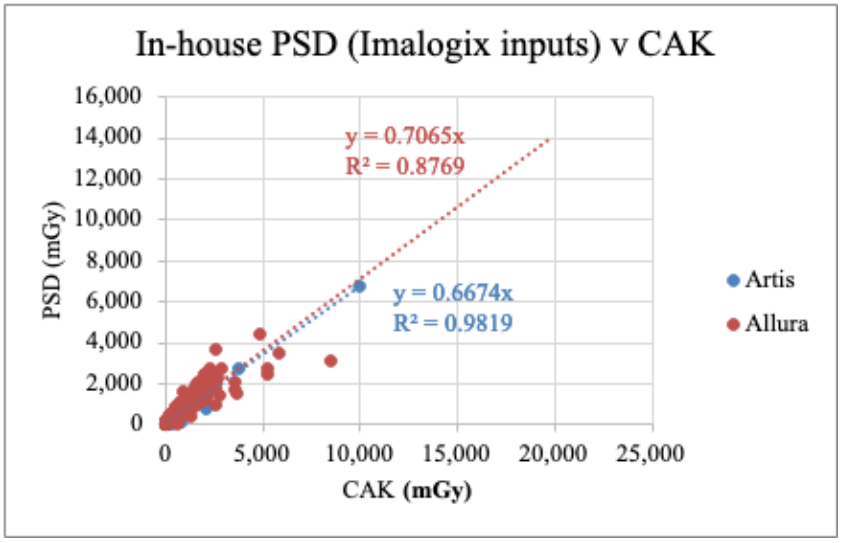

b)

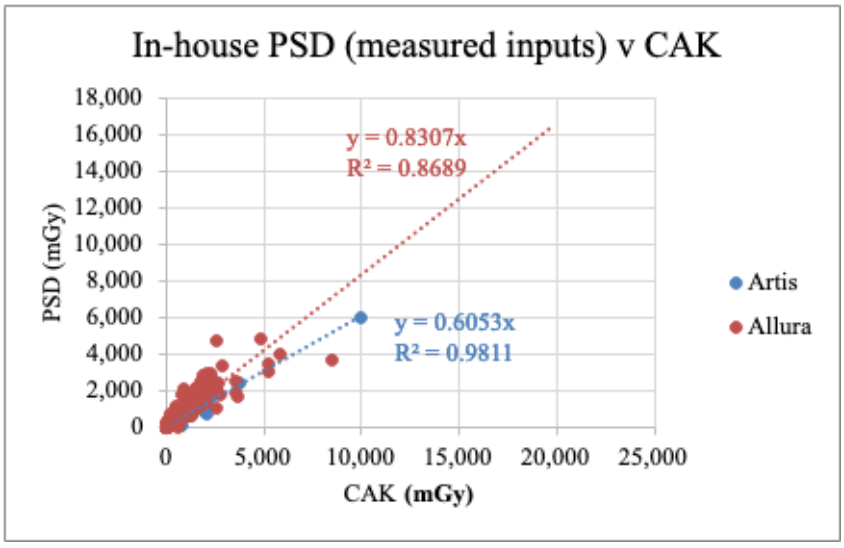

Figure 11. Imalogix and in-house PSD calculations compared uncorrected CAK using clinical RDSR data

a) In-house PSD calculations versus uncorrected CAK (Imalogix inputs)
b) In-house PSD calculations versus uncorrected CAK (measured inputs)

4.4. In-house PSD calculations vs. nanoDot measurements

RDSR data from the anthropomorphic phantom runs were used to test the in-house PSD calculator to nanoDot measurements; the results of this can be found in Figure 12. The

PSD calculation with $K_{a,r}$, BSF, and TAF values identical to Imalogix is labeled “In-house PSD (Imalogix inputs)”; the PSD calculation with corrected $K_{a,r}$ by testing year, measured BSF values, and measured TAF values are labeled “AK corr.”. Runs are separated by plane and independent variable tested; AP-FOV runs tested changing FOV with no table movement in the anterior-posterior plane, LAT-FOV runs tested changing FOV with no table movement in the lateral plane, and the FL-TAB tested table movement in the anterior-posterior plane using fluoroscopy mode. All runs were performed on the Siemens Artis Q unit.

The maximum nanoDot measurements from the anthropomorphic phantom runs can be found in Table 8. In the AP-FOV test runs, shown in Figure 12a) there was a consistent overestimation by Imalogix and close estimation by the in-house PSD calculator using corrections from the 2021 testing year. In the LAT-FOV test runs, shown in Figure 12b), there was a consistent underestimation by all PSD calculation methods. In the FL-TAB test runs, shown in Figure 12c), there was a consistent overestimation by Imalogix and close estimation by the in-house PSD calculator using corrections from the 2021 testing year. Dose distribution maps for PSD calculations, shown in Figure 13, are similar to those seen for the corresponding nanoDot measurements in Figure 9. Energy-corrected nanoDot dose distribution maps for anthropomorphic phantom runs. .

a)

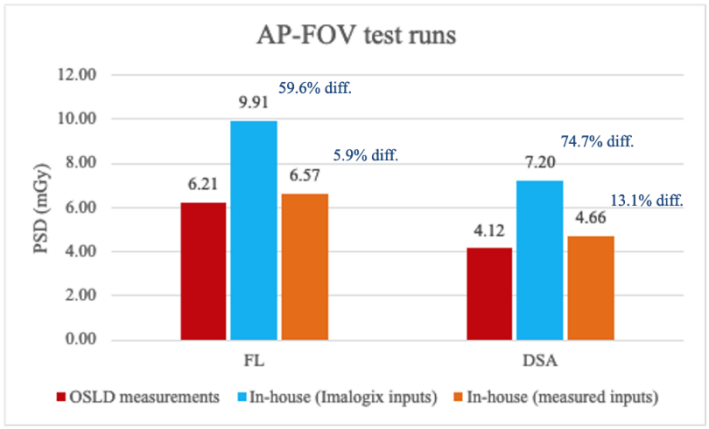

b)

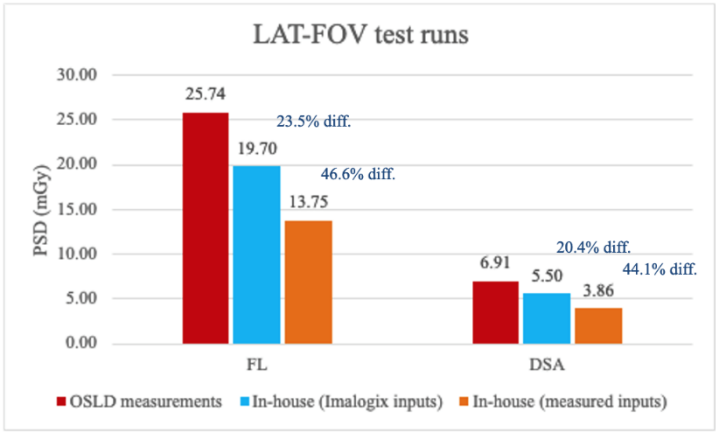

c)

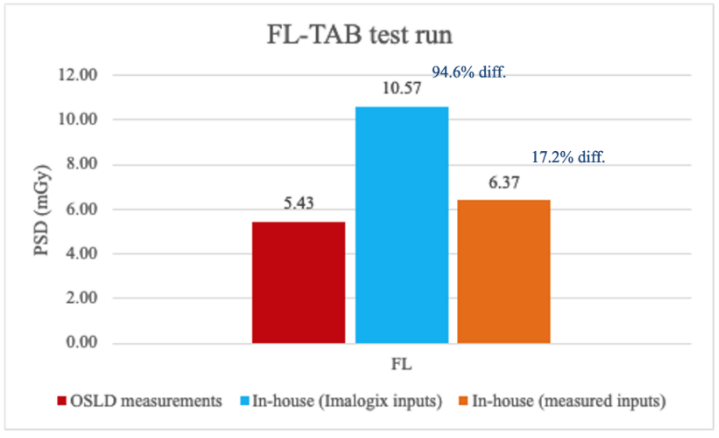

Figure 12. Various in-house PSD calculations as compared to nanoDot measurements on an anthropomorphic phantom.
a) Measured versus calculated PSD from AP-FOV test runs in fluoroscopy and DSA modes
b) Measured versus calculated PSD from LAT-FOV test runs in fluoroscopy and DSA modes
c) Measured versus calculated PSD from AP-plane table motion test runs in fluoroscopy mode

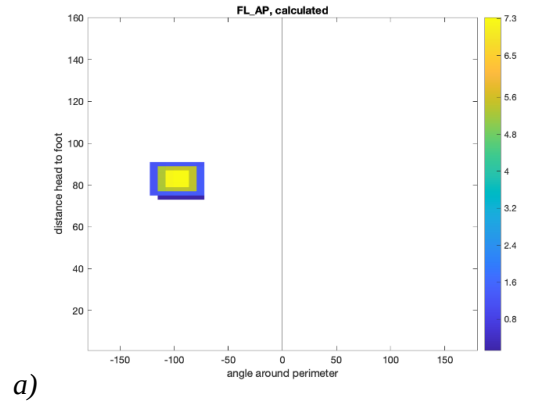

a)

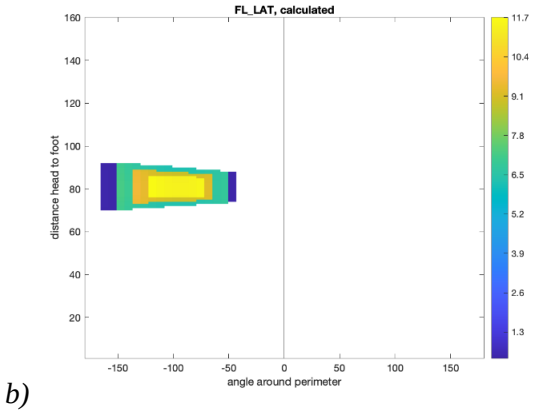

b)

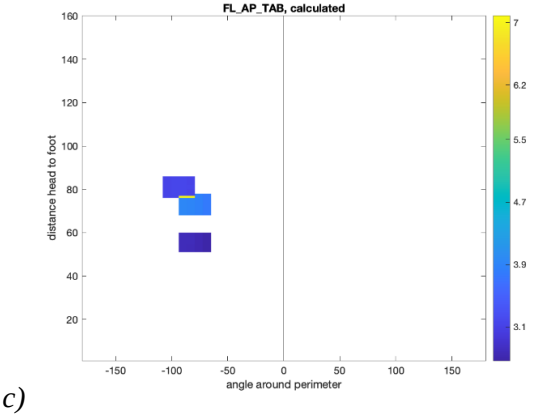

c)

Figure 13. Dose distribution maps created from in-house PSD calculator for test runs on an anthropomorphic phantom.

a) FL-AP run dose map calculated from RDSR; corresponding measured field in Figure 9. Energy-corrected nanoDot dose distribution maps for anthropomorphic phantom runs. *a.*
b) FL-LAT run dose map calculated from RDSR; corresponding measured field in Figure 9. Energy-corrected nanoDot dose distribution maps for anthropomorphic phantom runs. *b.*
c) FL-AP-TAB run dose map calculated from RDSR; corresponding measured field in Figure 9. Energy-corrected nanoDot dose distribution maps for anthropomorphic phantom runs. *c.*

5. Discussion

5.1. PSD variables

5.1.1. Air kerma

Many factors can be involved in the large range and annual change in $K_{a,r}$ meter accuracy. Examples include user-to-user equipment setup variability, tube replacements and or equipment output calibrations performed as part of PM duties, software updates, and dose reporting capabilities of the fluoroscopy units themselves. Although TG-190 outlines how to measure DAP- and $K_{a,r}$ meter accuracy, small variations in setup can present inaccuracies. It is important for field service engineers and physicists to be aware of setup at calibration and of any correction factors automatically adjusting for table presence. The percent error calculation requires CAK, which may display to whole units (1 mGy), making the calculation statistically imprecise for CAKs up to 10 mGy. Another factor that can introduce error is the definition for source-isocenter and source-reference point distance. Though data exists for this metric for the various vendor units, it often requires a literature search or searching through equipment operator manuals for exact technical specifications. To help minimize these errors, vendors should make source-reference distances easily retrievable and field service engineers should work alongside physicists during installation to confirm that Ka,r measurements and calibrations are performed under the same conditions. Providing step-by-step reference documents would be a great method of standardizing the measurement of this highly important PSD accuracy metric.

Assuming $K_{a,r}$ meter error is inherent to the x-ray tube, implementing a corrected $K_{a,r}$ can significantly improve the accuracy of a crude PSD estimate, as evidenced by the results

shown in Figure 12 a) and c), which showed over 50% reduction in percent difference when using corrected $K_{a,r}$. This applies to facilities with and without in-house physicists, as $K_{a,r}$ meter accuracy is already measured during annual testing. This may be especially meaningful for facilities that do not have dose tracking, as they likely have fewer physics resources and would have to spend more time on PSD calculation and potential notification or follow-up.

5.1.2. BSF

5.1.2.a. Philips Allura

The BSFs measured for the Philips Allura unit were found to match the range of those seen in the literature, as can be seen in Table 4 [7,9,10]. Because only two copper filtration thicknesses were measured, it was difficult to find a pattern with increasing copper filtration. The more apparent pattern, which was followed for all 0.1-mm and most 0.4-mm Cu runs, was increasing BSF with increasing FOV. This matches what is seen in the literature and is expected physically [7,9,10].

A major limitation of this measurement was lack of full control over the fluoroscopy unit; even in manual mode, one is unable to control or display the copper filtration. In order to take measurements at 0.1- and 0.4-mmCu, fluoroscopy and digital acquisition mode were utilized, respectively. Additionally, one meter in center of field may be insufficient for measuring BSF, as scatter in low-dose cases is unevenly distributed. If this unit were explored again, it would likely be done in manual mode using

radiochromic film to measure dose and a Piranha base unit to measure HVL.

5.1.2.b. Siemens Artis Q

The BSFs measured for the Siemens Artis Q unit were found to be smaller than those seen in the literature and had a narrower range, as can be seen in Table 5 [7,9,10]. The general increase then decrease in BSF with increasing copper filtration is akin to what is predicted by Jones & Pasciak [7]. Another expected pattern is for BSF to increase with increasing field size or FOV; this was apparent for most runs, as evidenced by the increasing BSF from 22- to 32-cm FOVs. Values in the 14-inches acrylic, 32-cm FOV, 0.3-mm Cu category were the only ones that did not follow this pattern. These values all fell below 1.10, indicating a possible error in measurement. Overall, BSF measurements used in the in-house calculation, i.e. those for 10-inches acrylic, followed expected patterns.

A major limitation of this measurement was lack of full control over the fluoroscopy unit; even in manual mode, there was uncertainty in the FOV setting. Manual mode on this unit allowed for control over applied copper filtration, which made measurements more predictable than those made on the Philips Allura unit. As mentioned in the previous subsection, one meter in center of field may be insufficient for measuring BSF, as scatter in low-dose cases is unevenly distributed. If this unit were explored again, it would likely be done as mentioned in the previous subsection: manual mode using radiochromic film to measure dose and a Piranha base unit to measure HVL.

5.1.3. TAF

5.1.3.a. Philips Allura

The TAFs measured on the Phillips Allura unit were found to have a wide range highly dependent on attenuator in the beam, as can be seen in Table 6. The additional attenuators tested are pictured in Figure 13. The thick gel tested was a “head donut” patient positioning device, the outer area of which resulted in a TAF of 0.34; if such a device were in-beam throughout the procedure, the resulting PSD would be vastly overestimated by a calculation that assumes a TAF of 0.75. Even the measured TAF for this unit used in the in-house PSD calculator, 0.77, would overestimate PSD in this scenario. To take these attenuators into account would require a strict record of when and where they are in-beam, which is not feasible. Because this results in an overestimation of PSD, however, it acts as a conservative estimate and is therefore clinically acceptable to assume a TAF equal to that of the table and pad. An underestimated PSD may result from a lateral-tube or bi-plane study, where the TAF should be equal to 1 due to no table between the beam and the patient. This is already taken into account by both Imalogix and the in-house PSD calculator, which sets TAF to 1 for C-arm rotational angles greater than 60 degrees.

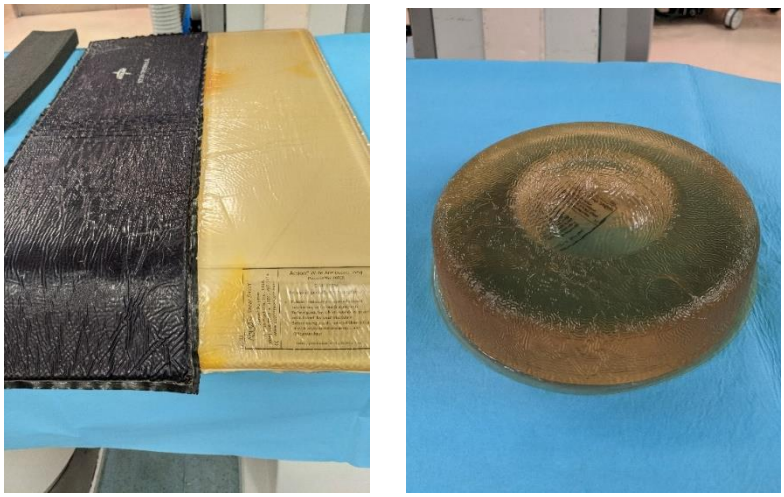

Figure 14. Photographs of thin (left) and thick (right) gel positioning devices used in Phillips Allura TAF measurements.

5.1.3.b. Siemens Artis Q

The TAF measured on the Siemens Artis Q unit was found to be equal to those assumed by Imalogix, as can be seen in Table 7. Due to time constraints, only the base attenuators, i.e. the table and pad, were explored. Additionally, as mentioned in the previous subsection, there is no record of what attenuators are clinically used let alone what is in the beam, so choosing a basic attenuation measurement is a sufficient assumption. If anything this would lead to an overestimation of PSD, as more attenuators lead to lower TAFs. Underestimation due to lateral x-ray tube positioning is avoided by setting TAF to 1 for C-arm rotational angles greater than 60 degrees.

5.2. nanoDot measurements

The nanoDot energy calibration, shown in Figure 8, was found to be reproducible by using both the T20 and Magna 1cc ion chamber and fit a linear curve that intersected 1.0 at 110 kVp. Landauer calibrates these to have a cross-over point at 80 kVp; the likely

reason for this is their calibration was performed at a beam quality of RQR6, which corresponds to 80 kVp at 3.0 mm Al filtration [14,15], whereas the beam filtration of the units in this study was likely between 3.2- and 3.4-mm Al. This underlines the importance of characterizing one's own set of nanoDots in-house prior to taking measurements; if the assumed characterization curve were used with a 1.0 crossover point at 80 kVp, nanoDot measurements would be incorrect by upwards of 10%. We, the authors, have no reason to believe that this characterization curve would not apply to the Siemens Artis Q unit although it was measured on the Phillips Allura unit. This could act as another limitation to the nanoDot anthropomorphic runs, especially if the HVL of the Siemens Artis Q unit was drastically different than the Philips Allura unit for the same kVp.

The first four test runs on the anthropomorphic phantom were limited to 8 x 8 cm^2 fields, which may or may not have contained the PSD location. FOV runs in the AP direction, shown by the dose distribution in Figure 9. Energy-corrected nanoDot dose distribution maps for anthropomorphic phantom runs. a), likely did contain the PSD, as corroborated by the similar-looking field in Figure 13a). FOV runs in the LAT direction, shown by the dose distribution in Figure 9. Energy-corrected nanoDot dose distribution maps for anthropomorphic phantom runs. b), likely did not contain the PSD; this could not be corroborated in Figure 13b). The final test run, which spanned a 25-cm field length and can be seen in Figure 9. Energy-corrected nanoDot dose distribution maps for anthropomorphic phantom runs. c), likely did contain the PSD, as corroborated by Figure 13c).

5.3. In-house PSD calculations vs. Imalogix PSD calculations

This version of the in-house PSD calculator was able to correlate to Imalogix at approximately 0.7 using the same inputs. This is likely due to a difference in RDSR variable interpretation or voxelized phantom geometry relative to the beam. Overall, the 0.7 correlation means that where Imalogix would result in a 6 Gy PSD, the in-house calculation would result in a 4 Gy PSD. Clinically, if the PSD alert level were set to 5 Gy, the in-house PSD calculation would fall below the notification limit, saving physician time and patient worry. However, neither of these has been tested in a clinical setting, meaning these are only with respect to each other. Figure 10 indicates only 1) how the in-house PSD calculator compares to Imalogix and 2) how much PSD varies using changing BSF and TAF as well as corrected air kerma. The in-house PSD versus CAK plots in Figure 11 show how different inputs change the relationship between PSD and uncorrected CAK. Inputting measured $K_{a,r}$, BSF, and TAF increased the slope of this line for the Philips Allura unit and decreased the slope for the Siemens Artis Q unit. This difference would most impact facilities that use CAK as a sole SRDL indicator prior to estimating PSD.

The implementation of $K_{a,r}$-accuracy into Imalogix PSD calculation would be simple and realistic. All that would be required would be a field for $K_{a,r}$ meter accuracy input by unit, which would be updated after annual testing, tube replacement, or system recalibration. This would scale CAK, DAP, and PSD by the inverse of one minus this percent error, either increasing or decreasing each of these by the same scale. It would be entirely up to

the user and Imalogix discretion as to whether or not this would be a useful correction to make and should be further validated with physical measurements.

Implementation of measured BSF and TAF values into a PSD calculator would require more effort on behalf of both the physicist and Imalogix. Rather, using constant values such as 1.3 for BSF and 0.75 for TAF are sensible for third-party dose monitoring systems such as Imalogix. If any implementation were to be made regarding these, it would be to measure an average BSF and TAF for each unit or fluoroscopy mode that could also be inputted to a field in Imalogix.

5.4. In-house PSD calculations vs. nanoDot measurements

From the AP test runs on an anthropomorphic phantom, it seems that the corrections applied to the in-house PSD calculator significantly closed the gap between measured and calculated values. Individual RDSRs from the test runs were unable to be submitted to Imalogix, but since Imalogix generally overestimates PSD as compared to the in-house calculation, as evidenced by Figure 10, it can be inferred that Imalogix PSD would be even greater than the in-house calculation using identical inputs and therefore further from measured PSD values. In a clinical scenario, the in-house PSD calculator would save unnecessary work and patient follow-up.

From the LAT test runs on an anthropomorphic phantom, it seems that the corrections applied to the in-house PSD calculator widened the gap between measured and calculated values. Individual RDSRs from the test runs were unable to be submitted into Imalogix,

but since Imalogix generally overestimates PSD as compared to the in-house program, as evidenced by Figure 10, it can be inferred that Imalogix PSD would be closer to measured PSD values. In a clinical scenario, the in-house program would underestimate the PSD, possibly leading to unchecked deterministic effects. Because of this, the in-house program needs to be re-evaluated for lateral beam applications.

6. Conclusions & Summary

6.1. Conclusions

Variables in a PSD calculation, specifically $K_{a,r}$, BSF, and TAF, were found to vary widely in this study. The $K_{a,r}$ meter accuracy meta-analysis showed that $K_{a,r}$ percent error should be incorporated into a PSD calculation due to the wide variability in $K_{a,r}$ accuracy, which was as large as 33% at OHSU between 2020 and 2021. Exposure rate measurements on the Philips Allura and Siemens Artis Q units examined resulted in BSFs between 1.16-1.77 and 1.08-1.36 and table/pad TAFs of 0.77 and 0.75, respectively. Measuring an average value per unit or per fluoroscopy mode would be another method of increasing PSD calculation accuracy.

The current version of the in-house PSD calculator correlates with Imalogix by approximately 0.7 using the same inputs; this gap is likely due to geometric discrepancies between the two programs. The in-house program, when using measured 2021 $K_{a,r}$ accuracy, BSFs, and TAFs, most closely matched OSLD measurements made on an anthropomorphic phantom in the AP plane. Because this program already estimates PSD 30% lower than Imalogix, it can be inferred that an Imalogix-calculated PSD would overestimate these measured values.

6.2. Limitations

Limitations of the BSF and TAF exposure rate measurements include lack of control over the fluoroscopic unit even in manual mode. This manifested itself as unknown and non-tunable copper filtration while in manual mode on the Philips Allura and possibly

changing FOV while in manual mode on the Siemens Artis Q. These could be checked through retrospective analysis of the RDSR data from measurement sessions. An additional limitation of the exposure rate measurements is the readable range of the T20 dose probe and Magna 1-cc ion chamber. Many of the exposure rates measured were on the scale of 0.01 mGy/s; the T20 is more suited for this than the Magna, which requires at least 0.25 mGy/s. In order to alleviate this, the experimental setup could be moved closer to the x-ray tube for increased exposure rate.

Another limitation of this work was the lack of Imalogix-calculated PSD for the OSLD-measured test runs. While the in-house calculation with Imalogix sufficed, it would have been beneficial to quantify the difference between calculated PSDs in this specific scenario. This highlights a common clinical limitation of PSD calculations: unsent exam RDSRs to Imalogix. Without the full RDSR, Imalogix is unable to calculate PSD, and the data point is lost. This impacted the retrospective analyses on PSD in this study and continues to complicate effective dose monitoring efforts at OHSU.

6.3. Future Work

In addition to implementing $K_{a,r}$ corrections into PSD calculations, working to improve $K_{a,r}$ meter accuracy will likely take place at OHSU. This process would include standardizing $K_{a,r}$ meter accuracy measurement methodology, verifying source-IRP distances, and working alongside vendors during x-ray tube calibrations. While error in displayed $K_{a,r}$ is technically acceptable up to 35%, it would be advantageous to any

institution to aim for accurate radiation dose metric displays, both for patient and personnel dose monitoring purposes.

Measured or calculated BSF values are scarce in the literature in the diagnostic energy range. Measuring full-field dose radiochromic film or performing Monte Carlo calculations to find BSF will translate well into future graduate student projects at OHSU. TAFs, although simple to measure, vary somewhat by x-ray techniques but more so by clinical attenuators used. It would be beneficial to interview clinicians or observe many FGIs in order to better understand which attenuators are used and when. In lieu of measuring TAFs for each room's attenuators, base measurements or Monte Carlo calculations could be performed.

As is already practice in some radiation oncology departments, nanoDots could be applied to patients undergoing high-dose procedures. There are a few concerns with this suggestion, namely the presence of a physicist to place, collect, and read these nanoDots, the likelihood that the nanoDots could miss the PSD location, and the use of small, non-sterile devices in an operating room, not to mention the energy dependence (+/- 10%) and angular dependence (+/- 40%) of the nanoDots [14,15]. Additionally, it is difficult to predict when an exam may lead to a high skin dose. This is not to say that direct measurements are impossible; nanoDots can be placed in sterile plastic cases and applied to the patient by a non-physicist, and for some case types it may be known in advance that high radiation exposure can be anticipated.

Further improving upon PSD calculation accuracy includes the consideration of complex geometries, a major example of which being biplane studies. Currently, the calculated PSD for these studies includes superimposing the two x-ray planes directly on top of each other for an ultra-conservative PSD estimate. Examining the geometry for each of the x-ray tubes and how they coordinate with each other would be of much clinical interest to biplane rooms with high-dose cases.

6.4. Summary

In order to monitor possible deterministic effects from an FGI, PSD is calculated. This value depends highly on $K_{a,r}$ meter accuracy, BSF, and TAF used. Imalogix, a dose monitoring software employed by OHSU, calculates PSD using on-unit $K_{a,r}$-meter readings and constant BSF and TAF values of 1.3 and 0.75, respectively. In this study, $K_{a,r}$ meter accuracy was found to be up to +/- 33% over all stationary fluoroscopic units at OHSU between 2020 and 2021, BSF was found to range from 1.06 to 1.77 between the two units studied, and TAF was found to range from 0.34 to 0.89 depending on attenuator used. When these factors were inputted into the in-house PSD calculator, PSD was closer to direct dosimetric measurements than when Imalogix inputs were used. By accounting for additional factors in PSD estimation, more accurate results can be achieved which translates to a more streamlined process for dose monitoring and patient follow-up care.

References

[1] NCRP (2010). National Council on Radiation Protection and Measurements. *Radiation dose management for fluoroscopically-guided interventional medical procedures*, NCRP Report No. 168 (National Council on Radiation Protection and Measurements, Bethesda, Maryland).

[2] IMV (2009). IMV Medical Information Division. *Benchmark Report, Cardiac Cath, 2008* (IMV Medical Information Division, Des Plaines, Illinois).

[3] IEC (2000). International Electrotechnical Commission. *Medical Electrical Equipment–Part 2-43: Particular Requirements for the Safety of X-Ray Equipment for Interventional Procedures*, IEC 60601-2-43 ed1.0 (International Electrotechnical Commission, Geneva).

[4] FDA (2009). U.S. Food and Drug Administration. "Performance standards for ionizing radiation emitting products. Fluoroscopic equipment," 21 CFR Part 1020.32, http://www.accessdata.fda.gov/scripts/cdrh/cfdocs/cfcfr/CFRSearch.cfm (U.S. Government Printing Office, Washington).

[5] IEC (2010). International Electrotechnical Commission. *Medical Electrical Equipment–Part 2-43: Particular Requirements for the Basic Safety and Essential Performance of X-Ray Equipment for Interventional Procedures*, IEC 60601-2-43 ed2.0 (International Electrotechnical Commission, Geneva).

[6] DICOM (2005). Digital Imaging and Communications in Medicine. *Supplement 94: Diagnostic X-Ray Radiation Dose Reporting (Dose SR)*, ftp://medical.nema.org/medical/dicom/final/sup94_ft.pdf (National Electrical Manufacturers Association, Rosslyn, Virginia).

[7] JONES, A.K. AND PASCIAK, A.S. (2011). "Calculating the peak skin dose resulting from fluoroscopically-guided interventions. Part I: Methods". *Journal of Applied Clinical Medical Physics* 12(4):231-244.

[8] AAPM (2015). American Association of Physicists in Medicine. *Accuracy and calibration of integrated radiation output indicators in diagnostic radiology*, AAPM Task Group Report No. 190 (American Association of Physicists in Medicine, Alexandria, VA).

[9] DELORENZO, M.C. & GOODE, A. R. (2019). "Evaluation of skin dose calculation factors in interventional fluoroscopy". *Journal of Applied Clinical Medical Physics* 20(12): 159-168.

[10] WUNDERLE, K.A., GODLEY, A.R., SHEN, Z.L., RAKOWSKI, J.T., DONG, F.F. (2017). "Percent depth doses and X-ray beam characterizations of a fluoroscopic system incorporating copper filtration". *Medical Physics* 44(4): 1275-1286.

[11] RTI (2016). "Piranha Reference Manual, v5.5H". RTI article number: 9629053-00. RTI Group AB.

[12] RTI (2019). "T20 Detector Data, v2019.12B". RTI article number: 9630514-00. RTI Group Headquarters.

[13] RTI (2020). "Magna 1cc A600 Ion Chamber, v2020.02a". RTI Group Headquarters.

[14] LANDAUER (2019a). "microSTAR®ii Medical Dosimetry System User Manual, v1.3". LANDAUER.

[15] LANDAUER (2019b). "microSTAR®ii and nanoDots FAQ". LANDAUER.